Supplemental Material

Supplementary Materials

Supplemental Text S1:
Arctic System Reanalysis – ASRv1

ASRv1 is an Arctic-specific regional reanalysis that utilizes the Eulerian non-hydrostatic Weather Research and Forecasting model version 3.3.1 (Polar WRF) (Skamarock et al. 2008), adapted for polar environments (Hines and Bromwich 2008) at a 30 km horizontal resolution for the period 2000-2012 (Bromwich et al. 2016). ASR uses a 3D-variational data assimilation scheme (Barker et al. 2004) wherein a forecast is produced every 3 hr and observations within +/- 1.5 hours of the forecast are used to produce the initial condition for the next forecast. The ASR forecast model uses the Goddard single-moment cloud microphysics scheme (Tao and Simpson 1993; Tao et al. 2003), which has prognostic variables for both cloud water and ice mixing ratios. ASR uses specified fractional sea ice coverage, sea ice thickness, snow cover, and albedo within each grid cell to calculate a surface energy balance, and is thus thought to be more sophisticated in the Arctic compared to other global reanalyses. ASRv1 more skillfully reproduces the state variables than ERA-Interim, but is not as accurate with the forecast variables such surface radiation fluxes and precipitation amounts.

National Centers for Environmental Prediction Reanalysis 1 - NCEP R1

NCEP R1is the first global climate reanalysis project to utilize a consistent model and assimilation system over an extended time period (Kalnay et al. 1996). It remains a widely-used reanalysis for Arctic research. NCEP R1 is produced at an approximate 2½° horizontal grid spacing (208 km) from 1948 to the present, and uses a 3D-variational data assimilation scheme that incorporates a 6-hr forecast model integration. For the period examined, sea ice boundary conditions are taken daily from NCEP passive microwave concentrations (Grumbine 1996), with an imposed threshold of 55% denoting a completely ice-free or ice-covered grid cell. Large-scale precipitation is based on the predicted model layer supersaturation. After accounting for evaporation in unsaturated, underlying layers, all precipitation penetrating the lowest layer is allowed to fall to the surface. It should be noted that NCEP R1 has been known to produce a spatial “ringing” effect for variables associated with high latitude moisture, owing to an oversimplification of the implemented diffusion equation (Kanamitsu et al, 2002).

National Centers for Environmental Prediction/Department of Energy Reanalysis 2 - NCEP R2

NCEP R2 is a global reanalysis with the same horizontal resolution as NCEP R1 (Kanamitsu et al. 2002). It was developed to address known issues in NCEP R1 – including the ringing effect – and incorporated subsequent model improvements, however NCEP R2 only covers the period from 1979 to the present. NCEP R2 uses the same 3D-variational data assimilation system as NCEP R1. Updates to the model physics largely concern the boundary layer diffusion, radiation, and the initialization of soil moisture (Kanamitsu et al. 2002).

National Centers for Environmental Prediction Climate Forecast System Reanalysis – CFSR

CFSR (Saha et al. 2010) is a global, weakly-coupled atmosphere, ocean, land, and sea ice analysis system with an approximate 0.3° (38 km) grid spacing, and was produced for the period 1979-2010. CFSR uses a 3D-variational data scheme with a 6-hr assimilation cycle. The

background model incorporates a dynamical ocean model with an interactive sea ice component. For the period examined, the initial sea ice concentration relies on both the NASA passive microwave product (Cavalieri et al. 1996) and the NCEP operational sea ice analyses (Wang et al. 2011; Wu and Grumbine 2013). The atmospheric model prognostically determines cloud water and ice mixing ratios using a simple microphysics scheme (Zhao and Carr 1997; Sundqvist et al. 1989). In the scheme, precipitation is determined via cloud condensate autoconversion parameterizations for liquid and ice (Moorthi et al. 2001).

European Centre for Medium-Range Weather Forecasts - ERA-Interim
ERA-Interim (Dee et al. 2011) is a global reanalysis with an approximate 0.7° (78 km) grid spacing, and covers the period 1979 to the present. The reanalysis uses a 4D-variational method with a 12-hr analysis cycle (Dee et al. 2011). Four different types of sea ice concentration data sets are used for the 2000-2016 period; these include the NCEP two-dimensional variational data assimilation until June 2001, weekly Optimum Interpolation SST Version 2 (Reynolds et al. 2002) (July-December 2001), NCEP real-time global daily SST (2002-April 2009), and the daily Operational Sea Surface Temperature and Sea Ice Analysis (OSTIA) product (Donlon et al. 2012). Model cloud microphysics, described in Tiedtke (1993), are based in part on the prognostic cloud condensate scheme of Sundqvist et al. (1989). Condensate phase is determined via a temperature threshold, and precipitation is diagnosed via an autoconversion parameterization.

Japanese 55-year ReAnalysis - JRA-55
JRA-55 (Kobayashi et al. 2015) is the Japan Meteorological Agency's second global atmospheric reanalysis, covering the period 1958 until the present at an approximate 0.6° (63 km) grid spacing. JRA-55 uses a 4D-variational assimilation system and provides forecasts every 6 hr. Sea ice cover is taken from microwave imager retrievals (Ishii et al. 2005). A threshold is applied in which the model grid cell is ice free for concentrations less than 55% and ice covered for values greater than 55%. A prognostic cloud condensate variable is maintained with the probability distribution methods of Smith (1990) and Sommeria and Deardorff (1977). Precipitation is diagnosed via autoconversion following Sundqvist (1998).

NASA's Modern-Era Retrospective Analysis for Research and Application - MERRA
MERRA is a global reanalysis produced by NASA's Global Modeling and Assimilation Office (GMAO)(Rienecker et al. 2011). MERRA was produced with the Goddard Earth Observing System Data Assimilation System (GEOS-DAS) at ½° grid spacing (74 km) between 1979 and February 2016. MERRA employed a 3D-variational assimilation system, as well as an incremental analysis update procedure (IAU) to correct the model to an observed state on a 6-hr analysis cycle (Bloom et al. 1996). Sea ice concentrations are obtained from weekly SST from Reynolds et al. (2002). As compared to the spectral global models in the other global reanalyses, the GEOS model is finite volume. The moist physics includes a prognostic cloud condensate as described in Bacmeister et al. (2006), which follows the autoconversion scheme of Sundqvist et al. (1989).

NASA's Modern-Era Retrospective Analysis for Research and Application, Version 2 – MERRA-2

MERRA-2 (Gelaro et al. 2017) is an update of the MERRA reanalysis system, with output fields available from 1980 to the present. MERRA-2 employs a constraint such that the globally-averaged net precipitation minus evaporation (P−E) equals the change in total atmospheric water (Takacs et al. 2016). This was designed to inhibit artificial jumps in precipitation associated with changes in the observing system, but is thought to have a negligible impact on high latitudes. As compared with MERRA, MERRA-2 employs an updated 3D-variational assimilation system with IAU, and has a comparable grid spacing of ½° (69 km) (Molod et al. 2015; Bosilovich et al. 2016). But prior to output, computations are performed on a cubed-sphere grid to better resolve Polar Regions. Sea ice concentrations use the daily SST product of Reynolds et al. (2007) until April 2006 and then OSTIA thereafter. For MERRA-2, the cloud parameterization of Bacmeister et al. (2006) includes large-scale condensation governed by a probability distribution function as described in Molod (2012).

Supplemental Text S2:
There are two events that stand out on days 285 and 310 when all six reanalyses show clear precipitation events, but the buoy shows no increase in snow depth. These discrepancies could be due to: (i) snowfall deposited on the sea ice getting blown off during windy conditions, or (ii), ice deformation in the immediate vicinity of the buoy that repositioned the buoy. Regarding the day 285 event, the buoy air pressure readings showed a dramatic increase from 996 hPa to 1032 hPa between Oct. 11 (day 284) and Oct. 12 (day 285) (**Fig. S5)**, which suggests that windy conditions were likely present and in line with Situation (i). For the event on day 310, we analyzed the raw IMB data from the top and bottom sonic rangefinders and thermistor strings to ascertain the cause for the discrepancy between the reanalysis and buoy results. The bottom sonic rangefinder recorded a ~11 cm downward drop in the position of the ice floe bottom over an 8-hour period, despite an increase in internal ice temperatures (**Fig. S6**). This coincides with a ~11 cm drop in the snow surface position, which was corrected during a prior quality check of the snow data. Air pressure readings also showed that a strong low pressure system had passed. Taken altogether, these results suggest that a deformation event occurred in the immediate vicinity of the buoy, which may have caused a physical repositioning of the buoy (and its sonic rangefinders), leading to a "missed" snowfall event described by Situation (ii).

Supplemental Text S3:
The reanalyses snowfall events (Fig. S3a) are clustered at times where there is a large increase in snow depth, but again the spread in the magnitude is quite large. Four of the reanalyses show a snowfall event around May 25 (day 145), where the buoy shows a decrease in snow depth. During the summer months when there is above freezing temperatures, JRA-55, MERRA and MERRA-2 all produce snowfall. ERA-Interim, on the other hand, produced almost no snowfall in the summer months, producing mostly rainfall (Fig. S3b), coinciding with above freezing air temperatures. ERA-Interim and JRA-55 also produced some possible spurious rainfall on days 325 and 350 when temperatures are well below freezing, highlighting the difficulty in reproducing the correct phase of precipitation.

Supplemental Text S4:
There is no snowfall (Fig. S4a) reported during the times of air temperatures above freezing (and here rainfall is captured, Fig. S4b), except for MERRA and MERRA-2 around August 25 (day 237). The large decreases in snowfall in August are shown to coincide with rainfall events and

above freezing temperatures exacerbating melt. These reanalyses also produce rainfall when the temperatures are below freezing and snow is accumulating (day 245, ~ September 2) which could be actual freezing rainfall not detected by the buoy, erroneous freezing rainfall (Dutra et al. 2011), or both.

References

Bacmeister, J. T., M. J. Suarez, and F. R. Robertson, 2006: Rain Reevaporation, Boundary Layer-Convection Interactions, and Pacific Rainfall Patterns in the AGCM, *J. Atmos. Sci*., doi:10.1175/JAS3791.1.

Barker, D. M., W. Huang, Y.-R. Guo, A. J. Bourgeois, and Q. N. Xiao, 2004: A Three-Dimensional Variational Data Assimilation System for MM5: Implementation and Initial Results, *Mon. Wea. Rev.*, doi:10.1175/1520-0493(2004)132<0897:ATVDAS>2.0.CO;2.

Bloom, S., L. Takacs, A. DaSilva, and D. Ledvina, 1996: Data assimilation using incremental analysis updates, *Mon. Wea. Rev.*, **124**, 1256-1271, doi:10.1175/1520-0493(1996)124<1256:DAUIAU>2.0.CO;2.

Bosilovich, M. G. and Co-Authors, 2016: MERRA-2. Initial evaluation of the climate, in *Global Modeling and Data Assimilation*, Tech. Rep. Ser., vol. **43**, edited by R. D. Koster NASA/TM-2015-104606,139 pp., Goddard Space Flight Center, Greenbelt, Md.

Bromwich, D. H., A. B. Wilson, L. Bai, G. W. K. Moore, and P. Bauer, 2016: A comparison of the regional Arctic System Reanalysis and the global ERA-Interim Reanalysis for the Arctic, *Q. J. R. Meteorol. Soc.*, **142**, 644-658, doi: 10.1002/qj.2527.

Cavalieri, D. J., C. L. Parkinson, P. Gloersen, and H. J. Zwally, 1996: Sea Ice Concentrations from Nimbus-7 SMMR and DMSP SSM/I-SSMIS Passive Microwave Data, Version 1, NASA National Snow and Ice Data Center Distributed Active Archive Center, Boulder, Colo., doi:10.5067/8GQ8LZQVL0VL.

Dee, D. P., and Coauthors, 2011: The ERA-Interim reanalysis: Configuration and performance of the data assimilation system, *Quart. J. Roy. Meteor. Soc*., **137**, 553-597, doi:10.1002/qj.828.

Donlon, C. J., M. Martin, J. Stark, J. Roberts-Jones, E. Fiedler, and W. Wimmer, 2012: The Operational Sea Surface Temperature and Sea Ice Analysis (OSTIA) system, *Remote Sens. Environ*., **116**, 140–158, doi:10.1016/j.rse.2010.10.017.

Dutra, E., S. Kotlarski, P. Viterbo, G. Balsamo, P. M. A. Miranda, C. Schär, P. Bissolli, and T. Jonas, 2011: Snow cover sensitivity to horizontal resolution, parameterizations, and atmospheric forcing in a land surface model, *J. Geophys. Res.*, **116**, D21109, doi:10.1029/2011JD016061.

Gelaro, R., and Coauthors, 2017: The Modern-Era Retrospective Analysis for Research and Applications, version-2 (MERRA-2). *J. Climate*, **30**, 5419-5454, doi:10.1175/JCLI-D-16-0758.1

Hines K.M., and D. H. Bromwich, 2008: Development and testing of Polar WRF. Part I: Greenland ice sheet meteorology, *Mon. Weather Rev.*, **136**, 1971–1989, doi: 10.1175/2007MWR2112.1.

Ishii, M., A. Shouji, S. Sugimoto, and T. Matsumoto, 2005: Objective analyses of sea-surface temperature and marine meteorological variables for the 20th Century using ICOADS and the Kobe Collection, *Int. J. Climatol.*, **25**, 865-879, doi:10.1002/joc.1169.

Kalnay, E., and Coauthors, 1996: The NCEP/NCAR 40-Year Reanalysis Project, *Bull. Amer. Meteor. Soc.*, **77**, 437-471, doi:10.1175/1520-0477(1996)077<0437:TNYRP>2.0.CO;2.

Kanamitsu, M., W. Ebisuzaki, J. Woollen, S. -K. Yang, J. J. Hnilo, M. Fiorino, and G. L. Potter, 2002: NCEP-DOE AMIP-II Reanalysis (R-2), *Bull. Amer. Meteor. Soc.*, **83**, 1631-1643, doi:10.1175/BAMS-83-11-1631.

Kobayashi, S., Y. Ota, Y. Harada, A. Ebita, M. Moriya, H. Onoda, K. Onogi, H. Kamahori, C. Kobayashi, H., Endo, K. Miyaoka, and K. Takahashi, 2015: The JRA-55 Reanalysis: General Specifications and Basic Characteristics, *J. Meteorol. Soc. Japan*, **93**, 5-48, doi:10.2151/jmsj.2015-001.

Molod, A., 2012: Constraints on the profiles of total water PDF in AGCMs from AIRS and a high-resolution model, *J. Climate*, **25**, 8341–8352, doi:10.1175/JCLI-D-11-00412.1.

Molod, A., L. Takacs, M. Suarez, and J. Bacmeister, 2015: Development of the GEOS-5 atmospheric general circulation model. Evolution from MERRA to MERRA2, *Geosci. Model Dev.*, **8**(5), 1339–1356, doi:10.5194/gmd-8-1339-2015.

Moorthi, S., H. L. Pan, and P. Caplan, 2001: Changes to the 2001 NCEP operational MRF/AVN global analysis/forecast system, NWS Technical Procedures Bulletin, Ser. No. 484, 14 pp.

Reynolds, R. W., N. A. Rayner, T. M. Smith, D. C. Stokes, and Q. Wang, 2002: An improved in situ and satellite SST analysis for climate, *J. Climate*, **15**, 1609–1625, doi:10.1175/1520-0442(2002)015<1609:AIISAS>2.0.CO;2.

Reynolds, R. W., T. M. Smith, C. Liu, D. B. Chelton, K. S. Casey, and M. G. Schlax, 2007: Daily high-resolution-blended analyses for Sea Surface Temperature, *J. Climate*, **20**, 5473–5496, doi:10.1175/2007JCLI1824.1.

Rienecker, M. M., and Coauthors, 2011: MERRA. NASA's Modern-Era Retrospective Analysis for Research and Applications, *J. Climate*, **24**, 3624-3648, doi:10.1175/JCLI-D-11-00015.1.

Saha, S., and Coauthors, 2010: The NCEP Climate Forecast System Reanalysis, *Bull. Amer. Meteor. Soc.*, **91**, 1015–1057, doi:10.1175/2010BAMS3001.1.

Skamarock W.C., J. B. Klemp, J. Dudhia, D. Gill, D. Barker, M. Dudhia, X.-Y. Huang, W. Wang, and J. G. Powers, 2008: A description of the advanced research WRF version 3, Technical Note TN-475+STR. NCAR: Boulder, CO.

Smith, R. N. B., 1990: A scheme for predicting layer clouds and their water content in a general circulation model. *Q.J.R. Meteorol. Soc.*, **116**, 435-460, doi:10.1002/qj.49711649210.

Sundqvist, H., E. Berge, and J. E. Kristjánsson, 1989: Condensation and cloud studies with mesoscale numerical weather prediction model, *Mon. Wea. Rev.*, **117**, 1641-1757, doi:10.1175/1520-0493(1989)117<1641:CACPSW>2.0.CO;2.

Sundqvist, H., 1998: Parameterization of condensation and associated clouds in models for weather prediction and general simulation, in Physically-Based Modelling and Simulations of Climate and Climatic Change—Part I, edited by M. E. Schlesinger, pp. 433–461, D. Reidel, Dordrecht, Netherlands.

Sommeria, G. and J.W. Deardorff, 1977: Subgrid-scale condensation in models of nonprecipitating clouds, *J. Atmos. Sci.*, **34**, 344-355, doi:10.1175/1520-0469(1977)034<0344:SSCIMO>2.0.CO;2.

Takacs, L. L., M. J. Suárez, and R. Todling, 2016: Maintaining atmospheric mass and water balance in reanalyses, *Q.J.R. Meteor. Soc.*, **142**, 1565-1573, doi:10.1002/qj.2763.

Tao W.-K., and J. Simpson, 1993: The Goddard Cumulus Ensemble model. Part I. Model description, *Terr. Atmos. Ocean. Sci.*, **4**, 19 – 54.

Tao W-K, J. Simpson, D. Baker, M.-D. Chou, B. Ferrier, D. Johnson, A. Khain, S. Lang, B. Lynn, C.-L. Shie, D. Starr, C.-H. Sui, Y. Wang, and P. Wetzel, 2003: Microphysics, radiation and surface processes in the Goddard Cumulus Ensemble (GCE) model, *Meteorol. Atmos. Phys.*, **82**, 97 – 137.

Tiedtke, M., 1993: Representation of clouds in large-scale models, *Mon. Wea. Rev.*, **121**, 3040-3061, doi:10.1175/1520-0493(1993)121<3040:ROCILS>2.0.CO;2.

Wang, W., P. Xie, S.-H. Yoo, Y. Xue, A. Kumar, and X. Wu, 2011: An assessment of the surface climate in the NCEP climate forecast system reanalysis, *Clim. Dyn.*, **37**, 1601-1620, doi:10.1007/s00382-010-0935-7.

Wu, X., and R. Grumbine, 2013: Sea ice in the NCEP Climate Forecast System Reanalysis, Proc. 38th NOAA Annual Climate Diagnostics and Prediction Workshop, 21-24 October, College Park, Md., 8 pp.

Zhao, Q. Y., and F. H. Carr, 1997: A prognostic cloud scheme for operational NWP models. *Mon. Wea. Rev.*, **125**, 1931-1953, doi:10.1175/1520-0493(1997)125<1931:APCSFO>2.0.CO;2.

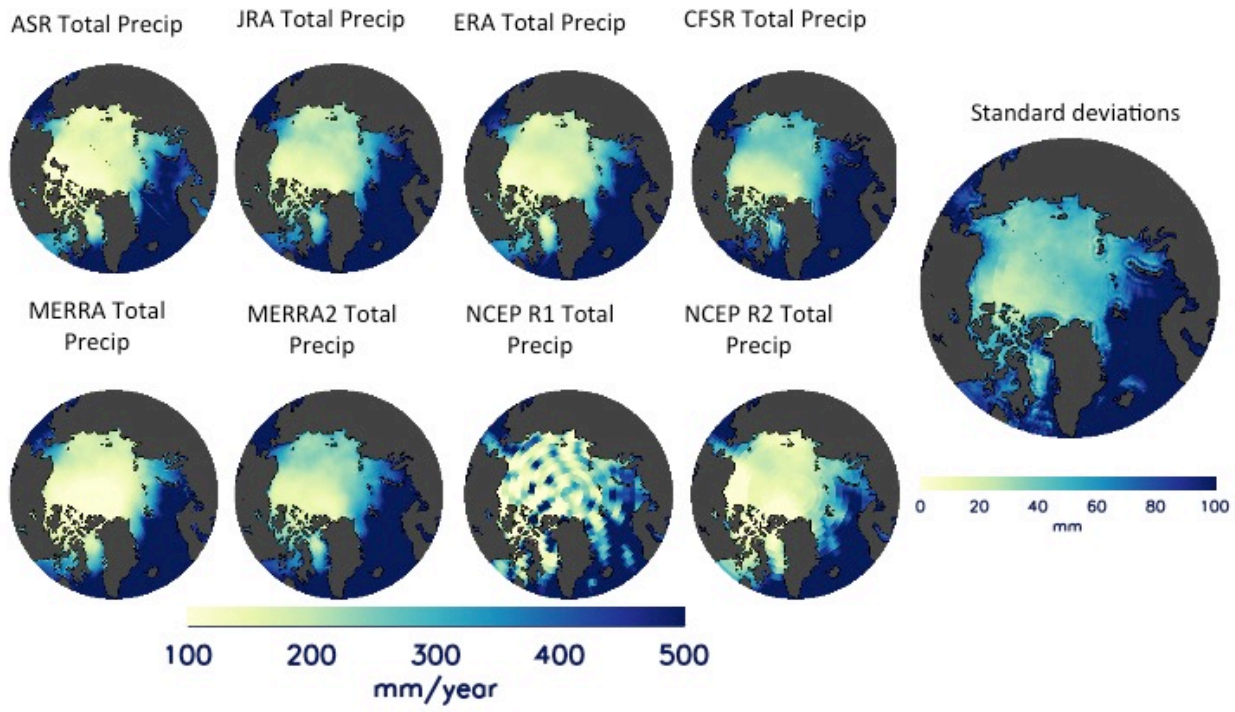

Supplemental Figure S1. Average annual 2000-2010 cumulative precipitation (Fig. 1) minus the average annual 2000-2010 cumulative trace precipitation where daily precipitation is less than 1mm day^{-1} (Fig. 10). The larger image shows the standard deviations between the 8 reanalyses in mm.

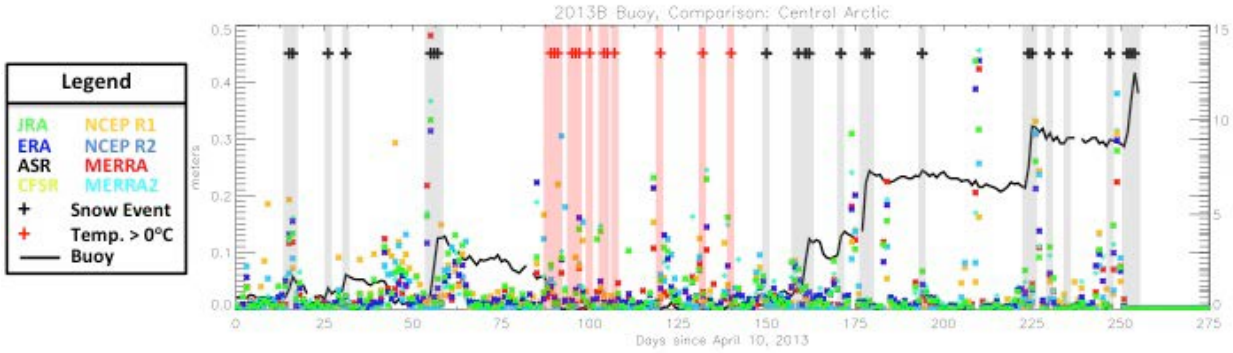

Supplementary Figure S2. 2013B IMB buoy (track shown in Fig. 2b) snow depth in meters (black line) beginning on April 10, 2013. Each color square represents the daily precipitation rate (mm day^{-1}, right axis) at the location of the buoy from each reanalysis. The black '+' and grey shaded boxes represent snowfall events. The red '+' and red shaded boxes represent times where the buoy recorded air temperatures above 0°C. *This figure includes the trace precipitation (less than 1 mm day^{-1}).*

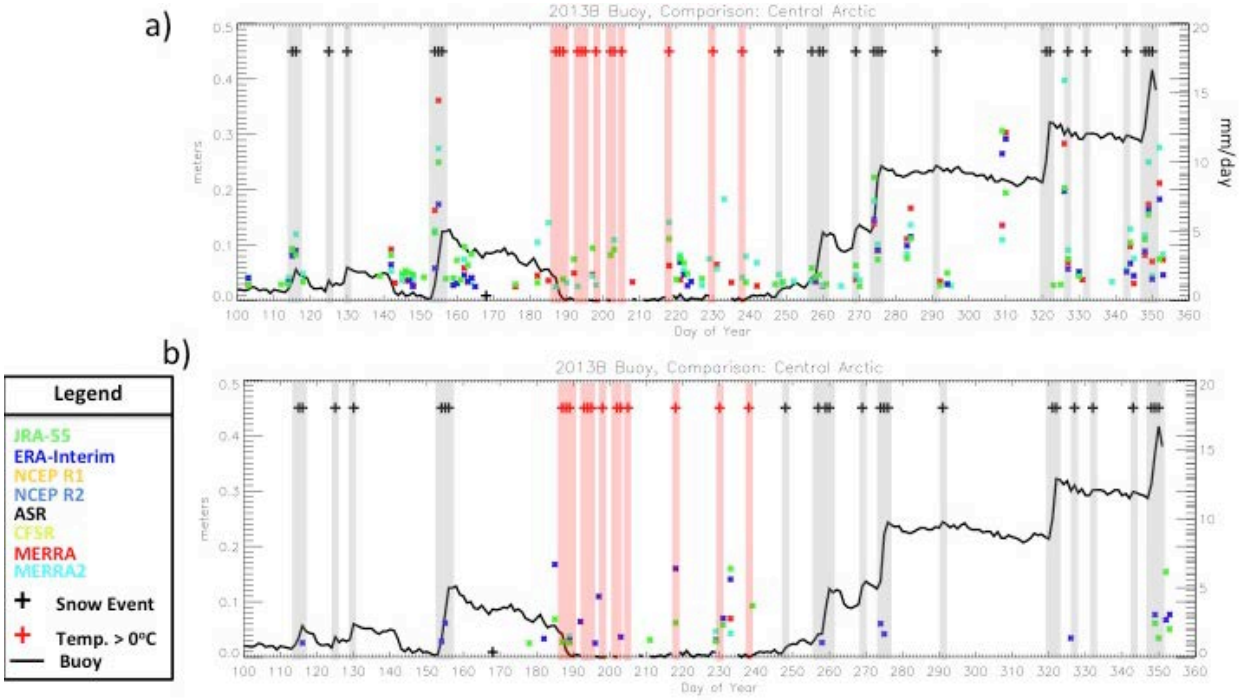

Supplementary Figure S3. 2013B IMB buoy (track shown in Fig. 2b) snow depth in meters (black line) beginning on April 10, 2013. Each color square represents the daily precipitation rate (mm day^{-1}, right axis) at the location of the buoy from each reanalysis. The black '+' and grey shaded boxes represent snowfall events. The red '+' and red shaded boxes represent times where the buoy recorded air temperatures above 0°C. a) Snowfall from four reanalyses (JRA-55, MERRA, MERRA-2, ERA-Interim). b) Rainfall from four reanalyses (same as for snowfall).

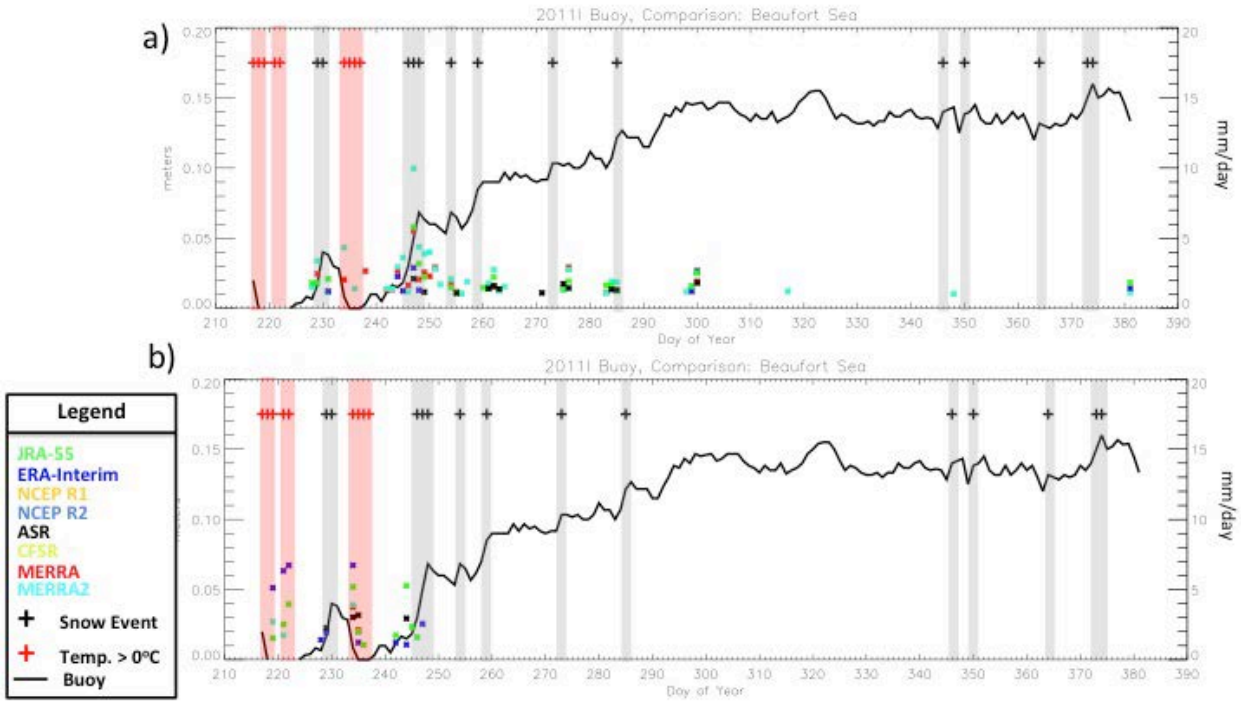

Supplementary Figure S4. 2011I IMB buoy (track shown in Fig. 2b) snow depth in meters (black line) beginning on August 17, 2011. Each color square represents the daily precipitation rate (mm day^{-1}, right axis) at the location of the buoy from each reanalysis. The black '+' and grey shaded boxes represent snowfall events. The red '+' and red shaded boxes represent times where the buoy recorded air temperatures above 0°C. a) Snowfall from four reanalyses (JRA-55, MERRA, MERRA-2, ERA-Interim). b) Rainfall from four reanalyses (same as for snowfall).

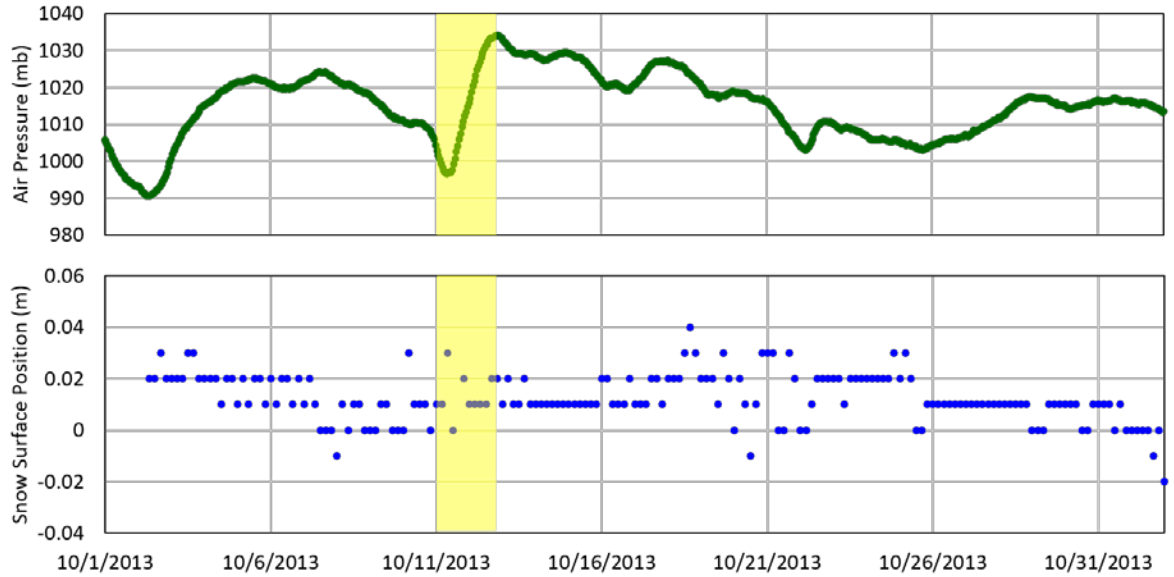

Supplementary Figure S5. IMB buoy 2013B daily air pressure (top) and snow surface position (bottom) for October 1-31, 2013. The highlighted box represents October 11-12 where are large pressure change associated with windy conditions lead to snow redistribution at the buoy.

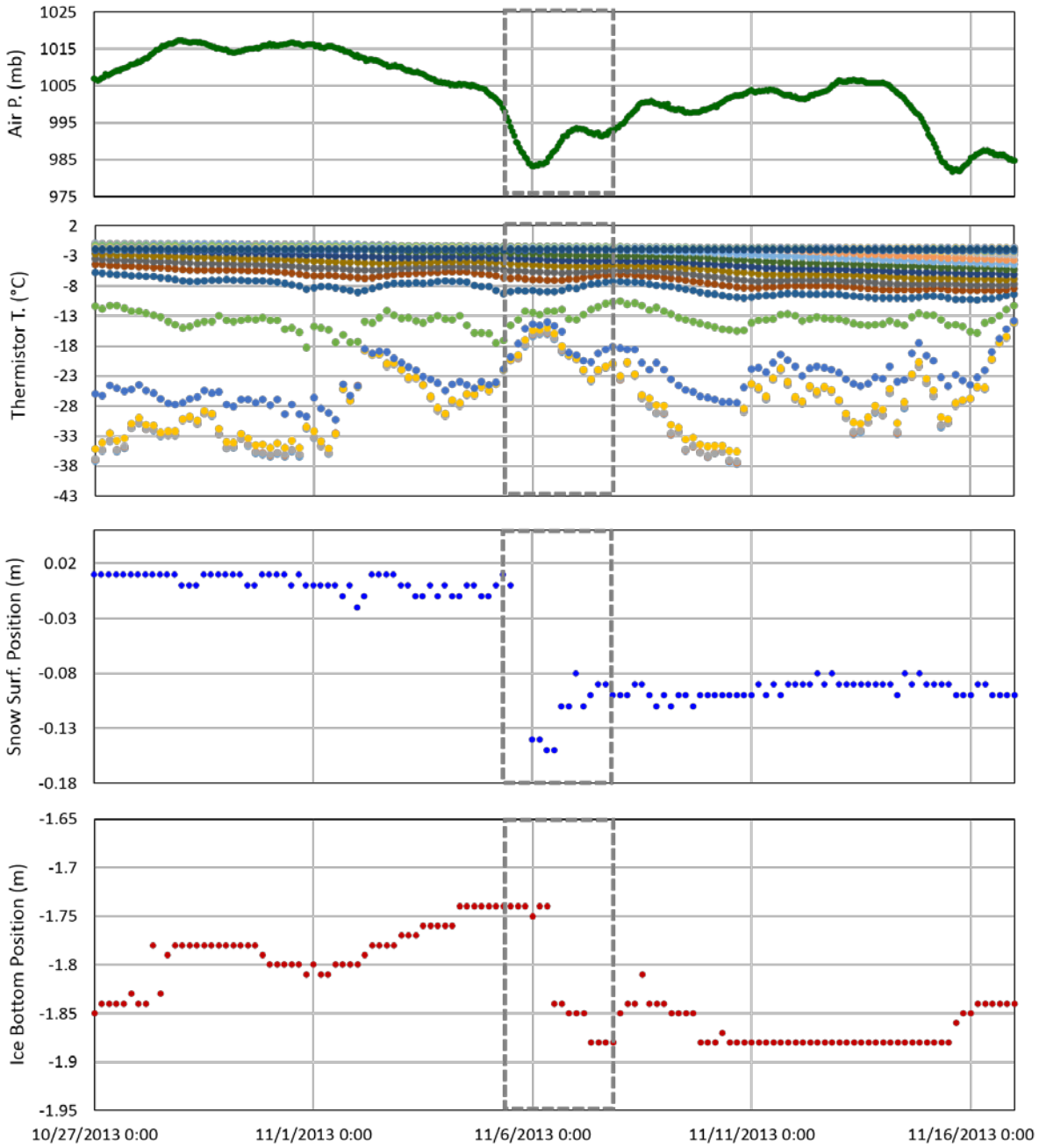

Supplementary Figure S6. IMB buoy 2013B air pressure, thermistor temperature (each color denotes a different point along the thermistor string), snow surface position, and ice bottom position for October 27-November 16. The event is highlighted by the grey dashed box**.**